

Supporting Information for

**Vanadium dissolution at 30°C and its suppression at low temperature
of -20°C for Na₃V_{1.5}Cr_{0.5}(PO₄)₃ cathode**

Yuxin Liao, Fushan Geng, Yu Jiang, Ming Shen, and Bingwen Hu*

**Shanghai Key Laboratory of Magnetic Resonance, State Key Laboratory of Precision Spectroscopy, School of Physics and Electronic Science, East China Normal University, Shanghai 200241, P. R. China*

Experimental

Material synthesis

$\text{Na}_3\text{V}_{1.5}\text{Cr}_{0.5}(\text{PO}_4)_3$ was synthesized using a typical sol-gel process. First, 0.03 mol of anhydrous citric acid was poured into 200 mL of deionized water and stirred rapidly at 80°C until complete dissolution. NH_4VO_3 (0.015 mol), $\text{Cr}(\text{NO}_3)_3$ (0.005 mol), Na_2CO_3 (0.015 mol), and $(\text{NH}_4)_2\text{H}_2\text{PO}_4$ (0.03 mol) were then added at intervals of 0.5 h, and a homogeneous solution was obtained after stirring for 1 h. The solution was then continuously stirred at 80°C until the water evaporated to dryness and the sol was obtained. The sol was then dried at 110°C for 12 h under vacuum to yield the gel. Finally, the gel mucosa was sintered to a powder, with the pristine $\text{Na}_3\text{V}_{1.5}\text{Cr}_{0.5}(\text{PO}_4)_3$ obtained via sintering at 350 and 800°C for 4 and 10 h, respectively.

Characterizations

X-Ray diffraction (XRD) of $\text{Na}_3\text{V}_{1.5}\text{Cr}_{0.5}(\text{PO}_4)_3$ was performed using a SmartLab SE diffractometer (Rigaku, Tokyo, Japan) with $\text{CuK}\alpha$ radiation ($\lambda = 1.5406 \text{ \AA}$). The pattern was collected in the 2θ range 10°–90° at a scan rate of 0.5°/min with a step size of 0.02°. The XRD patterns of the samples in different charging and discharging states were obtained using this instrument – the electrodes in their respective states were washed with dimethyl carbonate (DMC), and the adhered electrolyte on the surfaces was completely removed.

The contents of the V ions in the separators were determined using inductively coupled plasma-mass spectrometry (ICP-MS, Thermo Fisher Scientific, Waltham, MA, USA). The separators were extracted from the coin cells and soaked in 5 mL of 2 M KOH aqueous solution at 70°C for 12 h to fully extract the V ions, as V is an amphoteric metal. Deionized water (5 mL) was then added to the solution prior to centrifugation to remove the residual insoluble components of the glass fiber separators. The clear solution (5 mL) was further transferred to a glass bottle with a pipette and diluted to 10 mL prior to ICP-MS.

Electrochemical studies

The working electrodes were prepared by mixing the active material, super P conductive agent, and polyvinylidene difluoride in a mass ratio of 8:1:1 with drops of

N-methyl-2-pyrrolidone. The slurry was then coated onto Al foil and dried overnight at 110°C under vacuum. The mass loading of active material in each electrode was approximately 1.2 mg cm⁻². For in-situ XRD, 25–30 mg of the active mixture was loaded into our in-situ cell behind an Al-protected Be window. CR2032 coin-type cells were assembled in an Ar-filled glovebox, with O₂ and H₂O concentrations of <1 ppm, using the prepared working electrodes, metallic Na disks, separators (glass fiber filters), and 1 M NaClO₄ dissolved in EC:PC (1:1 v/v) as the electrolyte. Galvanostatic charge and discharge studies were conducted using a Land M340A_V5C100MT8 auto-cycler (Wuhan LAND Electronic, Wuhan, China). The working electrodes at different states of charge were extracted from the coin cells carefully inside the glove box and washed with DMC to remove the residual electrolyte. For the galvanostatic intermittent titration technique, the cells were charged at a current density of 20 mA/g for 15 min, followed by open-circuit relaxation for 10 h.

Solid-state nuclear magnetic resonance (NMR)

The ²³Na magic-angle spinning (MAS) NMR studies were conducted using a 400 MHz AVANCE III spectrometer (Bruker), operating at a ²³Na Larmor frequency of 105.84 MHz with a commercial triple-resonance 1.9 mm MAS probe. The ²³Na chemical shift was referenced to that of solid NaCl powder (7.2 ppm).

Preparation of the charged or discharged samples: Coin cells were carefully disassembled without short circuiting. Every removed electrode was then rinsed 6 times with DMC, soaked in 3 mL DMC for 3 h, and finally dried naturally to remove the residual electrolyte. The cycled materials were carefully scraped from the Al foil and used to fill 1.9 mm zirconia rotors. All operations were conducted in the Ar-filled glovebox.

of the V^{3+}/V^{4+} redox plateau (~ 3.4 V) in $\text{Na}_3\text{V}_2(\text{PO}_4)_3$ decreases significantly with increasing charge–discharge cycling. At the 15th discharge cycle, the specific capacity is only approximately 20 mAh g^{-1} , but for $\text{Na}_3\text{V}_{1.5}\text{Cr}_{0.5}(\text{PO}_4)_3$ (Figure S1d), the V^{3+}/V^{4+} redox plateau still maintains a specific capacity of ~ 60 mAh g^{-1} at the 30th charge–discharge cycle. Comparing Figures S1e and S1f shows that when $\text{Na}_3\text{V}_2(\text{PO}_4)_3$ is charged and discharged at different rates, the specific capacity changes drastically, e.g., when charging and discharging at a current of 0.1 C (10 mA/g), a specific capacity of 170 mAh g^{-1} is observed, but specific capacities of only 60, 20, and 0 mAh g^{-1} are observed at 0.3, 0.5, and 1 C, respectively. Additionally, upon returning to charging and discharging at 0.1 C, the specific capacity decreases rapidly. For $\text{Na}_3\text{V}_{1.5}\text{Cr}_{0.5}(\text{PO}_4)_3$, the differences in charge–discharge specific capacities at different rates are far smaller than those of $\text{Na}_3\text{V}_2(\text{PO}_4)_3$, e.g., at 0.5 C, a specific capacity of 110 mAh g^{-1} is still observed, and even at 1 C, stable charge–discharge with a specific capacity of 90 mAh g^{-1} is observed. Therefore, the introduction of Cr considerably improves the rate capability of $\text{Na}_3\text{V}_2(\text{PO}_4)_3$.

a) 30 °C , 2.5 – 3.6 V b) 30 °C , 1.0 – 3.6 V c) -20 °C , 1.0 – 3.9 V

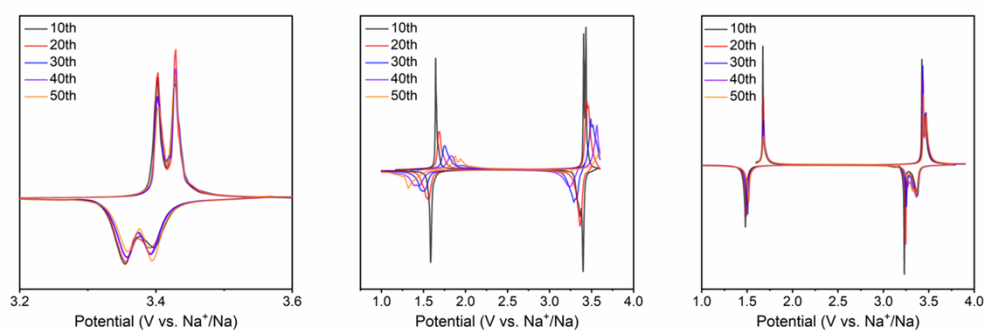


Figure. S2 dQ/dV patterns of $\text{Na}_3\text{V}_{1.5}\text{Cr}_{0.5}(\text{PO}_4)_3$ at 30°C within the potential window of (a) 2.5-3.6V and (b) 1.0-3.6V and (c) within the potential window of 1.0-3.9V at -20°C.

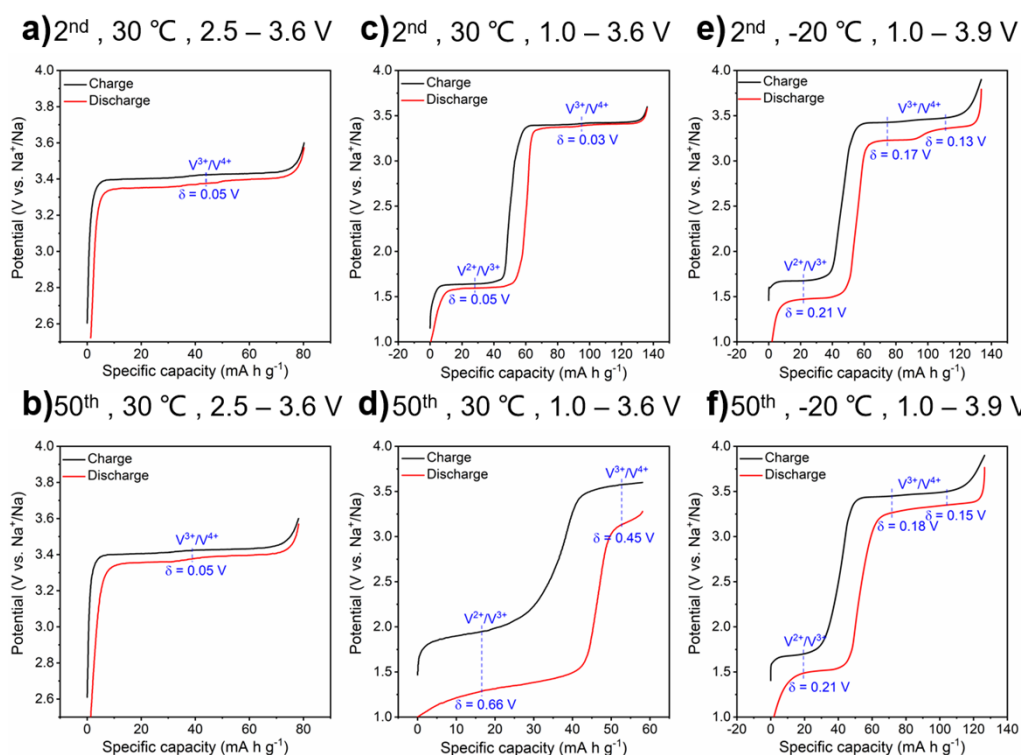


Figure. S3 Potential hysteresis curves of $\text{Na}_3\text{V}_{1.5}\text{Cr}_{0.5}(\text{PO}_4)_3$ at 30°C within the potential ranges of 2.5 - 3.6 V at (a) 2nd and (b) 50th cycle, within the potential ranges of 1.0 - 3.6 V at (a) 2nd and (b) 50th cycle, and at -20°C within the potential ranges of 1.0 - 3.9 V at (a) 2nd and (b) 50th cycle.

The potential hysteresis was compared for different testing conditions for the 2nd cycle and 50th cycle. Here 2nd cycle was used instead of 1st cycle because potential hysteresis curve of 2nd cycle should show the potential hysteresis at low voltage and two hysteresis curves for 1st cycle and 2nd cycle are almost identical.

At 30°C within the potential window of 2.5-3.6 V, the potential hysteresis of the plateaus corresponding to $\text{V}^{3+}/\text{V}^{4+}$ in the 2nd and 50th cycles (Figure S3a and S3b) are 0.05 and 0.05 V, respectively. Thus, under this condition, the potential hysteresis of NVCrP does not change significantly with increasing charge-discharge cycling. Within the potential window of 1.0-3.6 V, the potential hysteresis in the 2nd cycle corresponding to $\text{V}^{3+}/\text{V}^{4+}$ and $\text{V}^{2+}/\text{V}^{3+}$ are 0.03 and 0.05V, respectively (Figure S3c). At the 50th cycle (Figure S3d), the potential hysteresis corresponding to $\text{V}^{3+}/\text{V}^{4+}$ and

V^{2+}/V^{3+} are 0.45 and 0.66 V, respectively, which are significantly higher than the corresponding values during the 2nd cycle (Figure S3c). Therefore, the introduction of the potential window of 1.0-2.5 V with V^{2+}/V^{3+} redox at 30 °C leads to a significant increase in the potential hysteresis of NVCrP with increasing charge-discharge cycling.

At -20 °C within the potential window of 1.0-3.9 V, as shown in Figure S3e, although the potential hysteresis of 0.13, 0.17, and 0.21V for the 2nd cycle of NVCrP is larger than that at 30 °C (0.03 and 0.05V), but in the subsequent charge-discharge cycles, the change in the potential hysteresis is very small of ~0.01V, which indicates that the low temperature may effectively suppress the increase in the potential hysteresis of NVCrP.

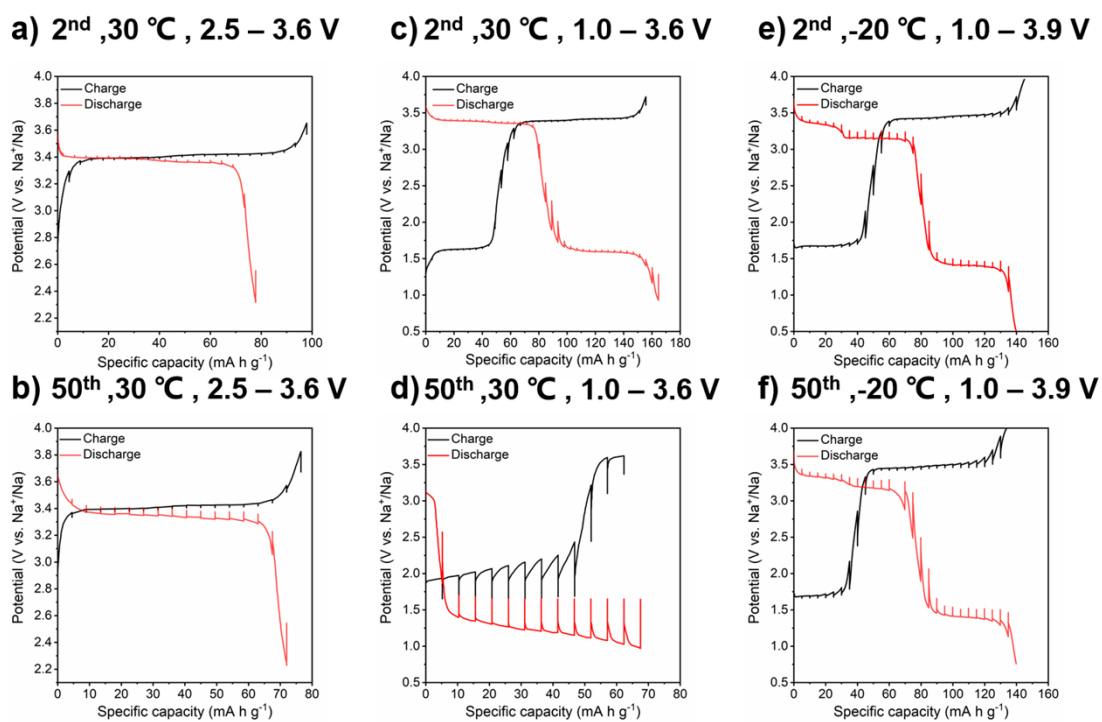


Figure. S4 Galvanostatic intermittent titration curves of $\text{Na}_3\text{V}_{1.5}\text{Cr}_{0.5}(\text{PO}_4)_3$ at 30 °C within the voltage range 2.5–3.6 V at the (a) 2nd and (b) 50th cycle, within the voltage range 1.0–3.6 V at the (c) 2nd and (d) 50th cycle, and at -20 °C within the voltage range 1.0–3.6 V at the (e) 2nd and (f) 50th cycle.

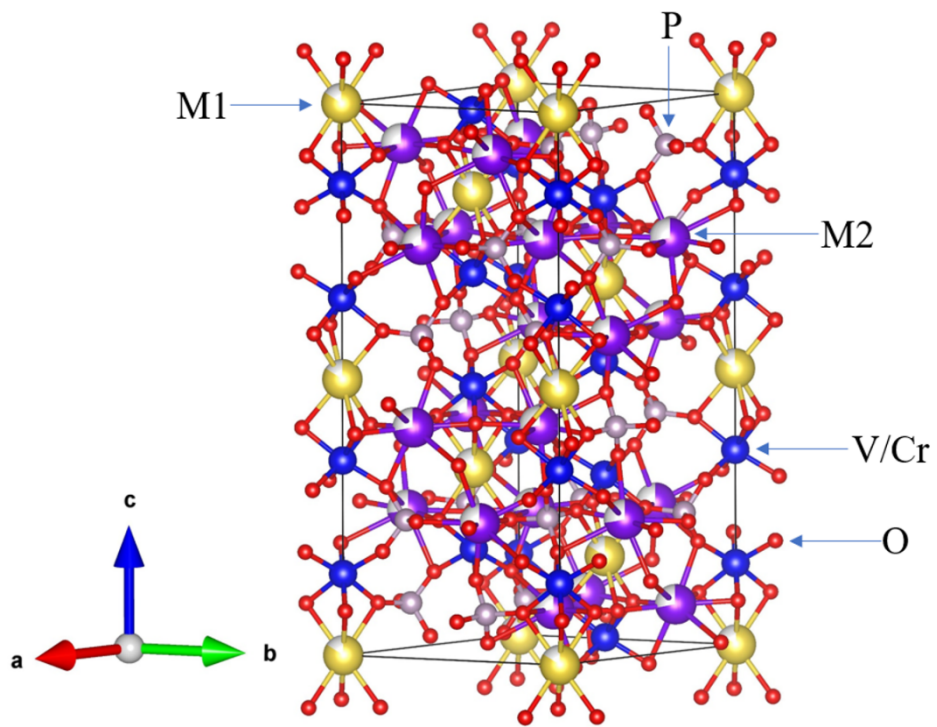


Figure S5. Structure of $\text{Na}_3\text{V}_{1.5}\text{Cr}_{0.5}(\text{PO}_4)_3$.

Notes and references

1. (a) X. Yao, Z. Zhu, Q. Li, X. Wang, X. Xu, J. Meng, W. Ren, X. Zhang, Y. Huang and L. Mai, *ACS Appl Mater Interfaces*, 2018, **10**, 10022-10028; (b) C. Wei, F. Luo, C. Zhang, H. Gao, J. Niu, W. Ma, Y. Bai and Z. Zhang, *Ionics*, 2019, **26**, 2343-2351; (c) Q. Wang, Y. Zhao, J. Gao, H. Geng, J. Li and H. Jin, *ACS Appl Mater Interfaces*, 2020, **12**, 50315-50323; (d) G. Li, Z. Yang, Y. Jiang, C. Jin, W. Huang, X. Ding and Y. Huang, *Nano Energy*, 2016, **25**, 211-217.